**SANDIA REPORT** SAND81-2521 • Unlimited Release • UC-~~94b~~
Printed December 1981

# Quasi-Static Rock Mechanics Data for Rocksalt from Three Strategic Petroleum Reserve Domes

Ronald H. Price, Wolfgang R. Wawersik, David W. Hannum,
Jeffrey A. Zirzow

**Prepared by**
**Sandia National Laboratories**
**Albuquerque, New Mexico 87185 and Livermore, California 94550**
**for the United States Department of Energy**
**under Contract DE-AC04-76DP00789**

## DISCLAIMER

Issued by Sandia National Laboratories, operated for the United States Department of Energy by Sandia Corporation.



Printed in the United States of America
Available from
National Technical Information Service
U.S. Department of Commerce
5285 Port Royal Road
Springfield, VA 22161

NTIS price codes
Printed copy: $6.00
Microfiche copy: A01

SAND--81-2521

SAND81-
Unlimited

DE82 006869

# QUASI-STATIC ROCK MECHANICS DATA FOR ROCKSALT FROM THREE STRATEGIC PETROLEUM RESERVE DOMES*

Ronald H. Price, Wolfgang R. Wawersik, David W. Hannum & Jeffrey A. Zirzow
Sandia National Laboratories**
Albuquerque, New Mexico 87185

## ABSTRACT

Triaxial compression and extension experiments have been run on rocksalt samples from three Strategic Petroleum Reserve (SPR) domes. Seventeen quasi-static tests were loaded at mean stress rates of .66-1.04 psi/sec (4.5-7.2 kPa/sec), confining pressures of 14.5-2000 psi (0.1-13.8 MPa) and temperatures of 22-100°C. Eleven of the test specimens were from Bryan Mound, Texas, and three each were from Bayou Choctaw, Louisiana, and West Hackberry, Louisiana.

In general, the resulting mechanical data from the three domes are similar, and they are consistent with previously published data. Ultimate sample strengths are directly related to confining pressure (least principal stress) and indirectly related to temperature, while ductility increases with both pressure and temperature.



* This work was supported by the U. S. Department of Energy (DOE) under Contract DE-AC04-76-DP00789.

** A U. S. DOE Facility.

TABLE OF CONTENTS


| | Page |
|---|---|
| List of Symbols and Conventions | 5-6 |
| List of Tables | 7-8 |
| List of Figures | 9-12 |
| Introduction | 13 |
| Site and Sample Description | 13 |
| General | 13 |
| Bayou Choctaw | 14 |
| Bryan Mound | 14 |
| West Hackberry | 15 |
| Experimental Techniques | 15 |
| Sample Preparation | 15 |
| Testing Apparatus and Procedures | 15 |
| Experimental Results | 17 |
| Test Conditions | 17 |
| Test Data | 17 |
| Summary and Conclusions | 24 |
| References | 25 |

## LIST OF SYMBOLS AND CONVENTIONS

| | |
|---|---|
| $\sigma_1$, $\sigma_2$, $\sigma_3$ | True principal stresses (force/current area); compressive stresses are positive |
| $e_1$, $e_2$, $e_3$ | Natural or logarithmic principal strains (change in length/current length); compressive strains are positive |
| $e = e_1 + e_2 + e_3$ | Volumetric strain |
| $\sigma_1 - \sigma_3$ | Principal stress difference or differential stress |
| $e_1 - e_3$ | Principal strain difference or differential strain |
| $(\sigma_1 - \sigma_3)_m$ | Maximum differential stress |
| $(\sigma_1 - \sigma_3)_u$ | Ultimate differential stress |
| $(e_1)_m$, $(-e_3)_m$, $(e_1 - e_3)_m$, $(e)_m$ | Natural strain values corresponding to $(\sigma_1 - \sigma_3)_m$ |
| E, $\nu$, G, K | Elastic moduli (Young's modulus, Poisson's ratio, shear modulus, bulk modulus) |
| T | Temperature |

Experimental data are given in both English and metric units, but are plotted in English units consistent with SPR project requests.

## LIST OF TABLES


| | | Page |
|---|---|---|
| Table I: | Matrix of Experiments ..... | 18 |
| Table II: | Test Data at Maximum Deviatoric Stress ..... | 20 |
| Table III: | Elastic (Unloading) Constants ..... | 21 |
| Table IV: | Mean Elastic Constants ..... | 23 |

## LIST OF FIGURES


| | | Page |
|---|---|---|
| Figure 1: | Loading Technique. Differential stress-time curve for sample BM 110A/2687 deformed in compression at 250 psi and 22°C .... | 26 |
| Figure 2: | Data Reproducibility. Differential stress-greatest principal strain, differential stress-differential strain and differential stress-volumetric strain curves for samples BC 19A/2581, BM 110A/2688.5 and BM 110B/3724 deformed in compression at 14.5 psi and 22°C ..... | 27-29 |
| Figure 3: | Effect of $\sigma_3$ in Compression. Differential stress-differential strain, differential stress-volumetric strain and differential strain-volumetric strain curves for samples WH 108/2294, WH 108/2291 and WH 108/2290 deformed in compression at 14.5, 500, 2000 psi and 60°C ..... | 30-32 |
| Figure 4: | Effect of $\sigma_3$ in Compression. Differential stress-differential strain, differential stress-volumetric strain and differential strain-volumetric strain curves for samples BM 110B/3728, BM 110B/3723 and BM 110A/2683.5 deformed in compression at 14.5, 500, 1500 psi and 100°C ..... | 33-35 |
| Figure 5: | Effect of $\sigma_3$ and T in Compression. Differential stress-differential strain and differential stress-volumetric strain curves for samples BM 110A/2688.5 and BM 110B/3728 deformed in compression at 14.5 psi and 22, 100°C; and BM 110A/2692 and BM 110A/2683.5 deformed in compression at 1500 psi and 22, 100°C ..... | 36-37 |
| Figure 6: | Effect of $\sigma_3$ in Extension. Differential stress-differential strain and differential stress-volumetric strain curves for samples BM 110A/2691 and BM 107C/2512 deformed in extension at 250, 500 psi and 22°C ..... | 38-39 |
| Figure 7: | Comparison of Compression and Extension. Differential stress-differential strain and differential stress-volumetric strain curves for sample WH 108/2291 deformed in compression and BC 19A/2579 deformed in extension at 500 psi and 60°C ..... | 40-41 |
| Figure 8: | Ultimate differential stress-least principal stress plots for samples deformed in compression and extension ..... | 42 |

LIST OF FIGURES (Cont'd.)


Page

Figure 9: Axial strain at $(\sigma_1 - \sigma_3)_u$-least principal stress plots for samples deformed in compression and extension ..... 43

Figure 10: Ultimate differential stress-temperature plots for samples deformed in compression and extension ..... 44

Figure 11: Axial strain at $(\sigma_1 - \sigma_3)_u$-temperature plots for samples deformed in compression and extension ..... 45

# QUASI-STATIC ROCK MECHANICS DATA FOR ROCKSALT FROM THREE STRATEGIC PETROLEUM RESERVE DOMES

Ronald H. Price, Wolfgang R. Wawersik, David W. Hannum & Jeffrey A. Zirzow
Sandia National Laboratories
Albuquerque, New Mexico 87185

## INTRODUCTION

The U. S. Strategic Petroleum Reserve (SPR) program is actively storing crude oil within salt domes along the Texas-Louisiana coastline. Mechanical properties on rocksalt are needed to aid in the design and certification of the storage caverns. In the latest series of short-term deformation experiments, seventeen samples from three separate SPR domes were tested under quasi-static loading conditions. These tests on Bayou Choctaw, Bryan Mound and West Hackberry core were designed to evaluate the effects of changes in confining pressure, temperature and loading conditions on mechanical behavior as a part of a long-range effort to (1) establish the mechanical response of rocksalt from different SPR sites and (2) assess the fracture potential of rocksalt within the walls of the storage caverns.

## SITE AND SAMPLE PREPARATION

### General

Bayou Choctaw, Bryan Mound, and West Hackberry domes are all diapiric structures formed from Jurassic salt rising into the Cenezoic sedimentary units of the Texas-Louisiana coastline along the Gulf of Mexico. The samples used in mechanical testing are from raw core approximately 4 in (10.2 cm) in diameter taken during drilling at potential cavern sites.

Bayou Choctaw (BC)

The Bayou Choctaw dome is located in Iberville Parish in south-central Louisiana. The large piercement structure is almost circular in horizontal cross-section. The three BC cores tested were from depths 2574-2581 ft (785.1-786.7 m) in drillhole 19A. All of the samples contained medium mean grain sizes of .31-.59 in (8-15 mm) with low standard deviations of .16-.28 in (4-7 mm). Although no chemical and mineralogical sample data were available, the samples appeared to be primarily (> 90%) halite (sodium chloride) with the predominant impurity probably being anhydrite. No preferential orientations of elongated grains or impurities were observed within any of these particular rocksalt specimens.

Bryan Mound (BM)

The Bryan Mound dome occurs within Brazoria County, Texas, one half mile from the coast of the Gulf of Mexico. This structure is also quite circular, with a relatively flat top at an approximate depth of 1100 ft (335 m). Experimental samples were obtained from the three drillholes 107C (1 sample), 110A (6) and 110B (4), at depth intervals of 2512 ft (756.6 m), 2683.5-2692 ft (817.9-820.5 m) and 3723-3728 ft (1135-1136 m), respectively. Grain sizes varied between .039 in (1 mm) and 1.7 in (43 mm) with an overall mean grain size of approximately .33 in (8.5 mm). Three samples (110A/2688.5, 110A/2692, 110B/3724) exhibited distinct color banding at very low angles to the specimen axes (i.e., approximately vertical). These dark and light gray anisotropies reflect variations in impurity content[1]. Mineralogical data from BM drillholes 107A, 107C, 108B and 109B reflect a halite content of at least 93%, with anhydrite as the dominant impurity ($\leq$ 6%)[1].

West Hackberry (WH)

West Hackberry dome is an irregularly shaped diapir located in Cameron Parish in southwestern Louisiana. The three WH test samples were from the depth interval 2290-2294 ft (698.0-699.2 m) in drillhole 108. Large variations in grain sizes (range: < .039-2.6 in; < 1-65 mm) were observed in all samples. No mineralogical data from these samples were available; however, these cores were the darkest of the cores tested, probably reflecting a higher concentration of impurities (perhaps up to 10% anhydrite). There were no preferred orientations of grains or impurities noted.

## EXPERIMENTAL TECHNIQUES

### Sample Preparation

All tests were performed on right circular cylinders. Raw cores were cut to an approximate length of 7.25-8.25 in (18.4-21.0 cm) on a band saw, then experimental samples were machined to desired diameter (compression samples: 3.5 or 4.0 in (8.9 or 10 cm); extension samples: 3.5 in (8.9 cm)) and a length of 7.0-8.0 in (18-20 cm). The specimen ends were machined flat and parallel to within ± 0.001 in (± .025 mm). The cores were turned using a tungsten carbide braze tool, Carboloy AX-8, Type 883. By using this technique, samples were obtained with sharp edges and minimal chipping or plucking of grains.

Prior to testing, all specimens were coated with a .01-.02 in (.25-.5 mm) thick layer of RTV silastic (RTV 108) to fill small surface pits. Each sample was then placed between vented steel end-caps and enclosed in a flexible jacket of Viton or Neoprene.

### Testing Apparatus and Procedures

All mechanical tests were conducted on two identical triaxial apparatus[2] that are designed for quasi-static and creep experiments both in triaxial

compression ($\sigma_1 > \sigma_2 = \sigma_3$) and triaxial extension ($\sigma_1 = \sigma_2 > \sigma_3$). These machines are capable of testing samples of up to 4.0 in (10.8 cm) in diameter and 8.25 in (21.0 cm) in length, at confining pressures up to 10.0 kpsi (69.0 MPa) and temperatures up to 250°C.

Axial forces were generated by a cylindrical, hydraulic ram, and measured by an external load cell. Fluid pressure was applied using silicone fluid and was monitored with standard transducers. Axial deformation of the sample was determined with two diametrically opposed LVDT's (linear variable differential transformers), by subtracting out the calibrated system deformations within the active gauge length. Lateral deformation was determined by means of one disk gauge[3] mounted at the central diameter along the specimen axis or measured dilatometrically. A detailed discussion of the techniques and data reduction procedures is given in an earlier report[4].

Once the samples were jacketed and placed in the vessel, the experimental sequence was initiated. For elevated temperature/pressure tests a hydrostatic confining pressure of 500 psi (3.4 MPa) was applied to the sample while the sample-vessel system was heated. When the appropriate test temperature was reached, the fluid pressure was changed to the desired experimental level. The deviatoric stress loading was then started by increasing either (1) the axial stress in a compression test or (2) the fluid pressure in an extension test. The loading paths were not smooth ramps, but a series of fast (< 2 sec) loading steps followed by four minutes of constant load. For every test, the initial stress increments were 250 psi (1.7 MPa). This loading technique resulted in an initial stress rate of 1.04 psi/sec (7.17 kpa/sec). Decreases in the stress rates of compression tests were caused by increases in specimen area with radial sample strain.

## EXPERIMENTAL RESULTS

### Test Conditions

The seventeen mechanical tests in this series included triaxial compression and extension experiments at mean stress rates of .66-1.04 psi/sec (4.5-7.2 kpa/sec), temperatures from 22 to 100°C and least principal stresses from 14.5 (atmospheric pressure) to 2000 psi (0.1 to 13.8 MPa). These ranges of pressures and temperatures were chosen since, under these conditions, rocksalt is pressure sensitive and prone to macroscopic failure. Table I is a matrix of experiments illustrating the specific sets of experimental conditions covered. The test/sample notation used in Table I and throughout this report consists of the following: dome, drillhole number/depth in feet (meters)/test type (C-compression, E-extension).

### Test Data

The reader should note that the data presented in this report, and that referred to from earlier studies, have not been segregated by domal site. This procedure appeared justified because the scatter in the results of samples from different locations was within that observed for samples from the same location deformed under identical conditions.

The experimental data curves are presented in Figures 1 through 7. Example plots of deviatoric stress versus time and versus axial strain are given in Figures 1 and 2A, respectively. The first graph illustrates the stepped loading path used in this test series. Figures 2B-7 are plots involving a combination of differential stress, differential strain and/or volumetric strain. The graphs have been chosen to exemplify (1) reproducibility of results (Figure 2), (2) effect of $\sigma_3$ changes in compression (Figures 3 and 4), (3) effect of $\sigma_3$ and T changes in compression

Table I

Matrix of Experiments

| Least Principal Stress (psi/MPa) | Temperature (°C) 22 | 60 | 100 |
|---|---|---|---|
| 14.5/0.10 | BC 19A/2581(786.7)/C<br>BM 110A/2688.5(819.4)/C<br>BM 110B/3724(1135.0)/C | WH 108/2294(699.2)/C | BM 110B/3728(1136.2)/C |
| 25C/1.72 | BM 110A/2687(819.0)/C<br>BM 110A/2691(820.2)/E | | |
| 500/3.45 | BM 107C/2512(765.6)/E | BC 19A/2579(786.0)/E<br>WH 108/2291(698.3)/C | BM 110A/2685(818.3)/C<br>BM 110B/3723(1134.7)/C |
| 1500/10.3 | BM 110A/2692(820.5)/C<br>BM 110B/3725(1135.6)/E | | BM 110A/2683.5(817.9)/C |
| 2000/13.8 | | BC 19A/2576(785.1)/E<br>WH 108/2290(698.0)/C | |

(Figure 5), (4) effect of $\sigma_3$ changes in extension (Figure 6) and (5) comparison of compression and extension at constant $\sigma_3$ and T (Figure 7). Test data at maximum differential stresses and the elastic constants are summarized in Tables II and III, respectively. Six samples tested did not reach ultimate strength (see Table II), and therefore the maximum value is given. The maximum differential stresses reported are the absolute peak stresses attained throughout the stepped loading history of each sample. The maximum strains correspond directly to the values at the maxmium differential stress.

The summary plots in Figures 8-11 illustrate the effects of $\sigma_3$ and T on differential stress and axial strain (i.e., greatest principal strain) in compression and extension. As noted on the graphs, most of the data points plotted are actual ultimate stresses and axial strains at failure. The maximum data are included for completeness, but are only lower bounds on the appropriate ultimate stresses and strains.

The experimental results presented here are consistent in trends and magnitudes with other published rocksalt data, including two earlier reports on domal rocksalt[5,6]. As shown in Figures 8 and 9, rocksalt is pressure sensitive in the 14.5-2000 psi (0.1-13.8 MPa) range. As expected, within the range of $\sigma_3$ values salt becomes distinctly stronger with increased least principal stress. Ductility (greatest principal strain to failure) is also directly related to $\sigma_3$. The effect of temperature on strength and ductility is shown in Figures 10 and 11. At atmospheric pressure, no trend of temperature dependence on strength is seen, while ductility increases slightly with temperature. However, at higher pressures (500 psi; 3.45 MPa and 1500 psi; 10.3 MPa), strength decreases with increasing temperature. In compression, ductility increases with temperature,

## Table II

### Test Data at Maximum Deviatoric Stress

| Test Sample Drillhole/Depth-Ft(m)/ Test Type | $\sigma_3$ psi(MPa) | T °C | $(\sigma_1 - \sigma_3)_m$ kpsi(MPa) | $(e_1)_m$ % | $(-e_3)_m$ % | $(e_1 - e_3)_m$ % | $(e)_m$ % |
|---|---|---|---|---|---|---|---|
| BC 19A/2581(786.7)/C | 14.5(0.1) | 22 | 3.74(25.8)* | 3.01 | 3.12 | 6.14 | -3.24 |
| BM 110A/2688.5(819.4)/C | 14.5(0.1) | 22 | 2.81(19.4)* | 2.02 | 3.00 | 5.02 | -3.99 |
| BM 110B/3724(1135.0)/C | 14.5(0.1) | 22 | 4.02(27.7)* | 3.10 | 4.51 | 7.60 | -5.91 |
| BM 110A/2687(819.0)/C | 250(1.72) | 22 | 6.05(41.7)* | 7.49 | 5.56 | 13.1 | -3.62 |
| BM 110A/2692(820.5)/C | 1500(10.3) | 22 | 9.54(65.8)* | 31.3 | 18.2 | 49.5 | -5.10 |
| WH 108/2294(699.2)/C | 14.5(0.1) | 60 | 3.79(26.1)* | 4.27 | 4.47 | 8.74 | -4.66 |
| WH 108/2291(698.3)/C | 500(3.45) | 60 | 5.78(39.9)* | 18.8 | 11.5 | 30.3 | -4.22 |
| WH 108/2290(698.0)/C | 2000(13.8) | 60 | 7.50(51.7) | 23.8 | 13.0 | 36.8 | -2.24 |
| BM 110B/3723(1136.2)/C | 14.5(0.1) | 100 | 3.74(25.8)* | 4.45 | 5.62 | 10.1 | -6.78 |
| BM 110A/2685(818.3)/C | 500(3.45) | 100 | 5.32(36.7)* | 23.6 | 15.2 | 38.9 | -6.77 |
| BM 110B/3723(1134.7)/C | 500(3.45) | 100 | 5.46(37.7)* | 23.2 | 14.1 | 37.3 | -5.12 |
| BM 110A/2683.5(817.9)/C | 1500(10.3) | 100 | 6.54(45.1) | 32.4 | 18.3 | 50.7 | -4.80 |
| BM 110A/2691(820.2)/E | 250(1.72) | 22 | 6.62(45.7) | 3.54 | 8.67 | 12.2 | -1.59 |
| BM 107C/2512(765.6)/E | 500(3.45) | 22 | 7.43(51.2)* | 5.22 | 9.61 | 14.8 | 0.830 |
| BM 110B/3726(1135.6)/E | 1500(10.3) | 22 | 8.46(58.3) | 6.27 | 12.1 | 18.4 | 0.421 |
| BC 19A/2579(786.0)/E | 500(3.45) | 60 | 4.98(34.3) | 3.49 | 7.29 | 10.8 | -0.305 |
| BC 19A/2576(785.1)/E | 2000(13.8) | 60 | 6.44(44.4) | 6.65 | 11.9 | 18.5 | 1.46 |

* Actual ultimate stress value.

Table III

Elastic (Unloading) Constants

| Test Sample Drillhole/Depth-Ft(m)/ Test Type | $\sigma_3$ psi(MPa) | T °C | E[a] Mpsi(GPa) | $\nu$[a] | G[b] Mpsi(GPa) | K[b] Mpsi(GPa) |
|---|---|---|---|---|---|---|
| BM 110A/2687(819.0)/C | 250(1.72) | 22 | 4.57(31.5) | .27 | 1.80(12.4) | 3.31(22.8) |
| BM 110A/2692(820.5)/C | 1500(10.3) | 22 | 5.36(37.0) | .31 | 2.05(14.1) | 4.70(32.5) |
| WH 108/2291(698.3)/C | 500(3.45) | 60 | 5.37(37.0) | .32 | 2.03(14.0) | 4.97(34.3) |
| WH 108/2290(698.0)/C | 2000(13.8) | 60 | 5.68(39.2) | .23 | 2.31(15.9) | 3.51(24.2) |
| BM 110A/2685(818.3)/C | 500(3.45) | 100 | 4.57(31.5) | .28 | 1.79(12.3) | 3.46(23.9) |
| BM 110B/3723(1134.7)/C | 500(3.45) | 100 | 4.92(33.9) | .28 | 1.92(13.2) | 3.73(25.7) |
| BM 110A/2683.5(817.9)/C | 1500(10.3) | 100 | 4.11(28.3) | .39 | 1.48(10.2) | 6.23(42.9) |
| BM 107C/2512(765.6)/E | 500(3.45) | 22 | 4.91(33.9) | .33 | 1.85(12.7) | 4.81(33.2) |

[a] measured

[b] calculated

as has been previously published. Equivalent data for extension are less complete. The ultimate differential stresses were reached in only two of four experiments; however, the same trend of decreasing strength and increasing ductility with temperature is suggested. Volumetric strain measurements are also influenced by least principal stress and temperature (see Table II). Dilatancy at fixed values of principal stress difference decreases as pressure and/or temperature is raised.

As an earlier report[6] discussed, there are marked differences between compression and extension results from tests at equivalent T and $\sigma_3$. In general, the extension samples are approximately the same strength, but reach far less greatest principal, differential and volumetric strains at failure than the compression samples. These contrasting results are attributed to distinctly different failure modes. All extension samples taken to failure broke suddenly along a single extension fracture (i.e., a fracture perpendicular to $\sigma_3$); whereas, the compression specimens tended to fail more stably by the formation of many mesoscopic (.5-3.0 in; 1.3-7.6 cm) shear and extension cracks preceding the loss of cohesion on one or more macroscopic shear fractures. The volumetric strain data presented here and from the two previous studies should prove to be significant in the development of a general fracture criterion for rocksalt.

The elastic (unloading) constants obtained in this test series are presented in Table III. The Young's moduli and Poisson's ratios fall within the ranges of values previously published. These experimentally measured values were used to calculate the shear and bulk moduli. By combining these data with those from two earlier reports[5,6], mean elastic constants were determined for Bryan Mound, West Hackberry and overall SPR rocksalt (Table IV). The stated value of E is 18 percent higher for West

Table IV

Mean Elastic Constants[a]

| Location | $E^b$ Mpsi (GPa) | $\nu^b$ — | $G^c$ Mpsi (GPa) | $K^c$ Mpsi (GPa) |
|---|---|---|---|---|
| Bryan Mound | 4.72 (32.6) | .33 | 1.77 (12.2) | 4.63 (31.9) |
| West Hackberry | 5.57 (38.4) | .30 | 2.14 (14.8) | 4.64 (32.0) |
| Overall | 4.94 (34.1) | .32 | 1.87 (12.9) | 4.57 (31.5) |

[a] Data from references 5 and 6 and this report.

[b] Mean of measured values.

[c] Calculated from E and $\nu$ values.

Hackberry than for Bryan Mound. This result may be due to West Hackberry samples containing a greater concentration of impurities (e.g., anhydrite) than the Bryan Mound material.

## SUMMARY AND CONCLUSIONS

Seventeen quasi-static experiments on rocksalt from three SPR sites have been presented. The test results were reproducible and consistent with previously published data. The minor variations in sample grain sizes and in composition did not appear to have an effect on strength and behavior trends. As expected, specimen strength was directly related to the least principal stress and inversely related to temperature; furthermore, pressure and temperature increases resulted in larger axial strains to failure (ductility). While strengths in extension and compression were similar, ultimate strains were substantially higher in compression than in extension.

## REFERENCES


1. Bild, R. W. (1980), "Chemistry and Mineralogy of Samples from the Strategic Petroleum Reserve Bryan Mound Site," Sandia National Laboratories Report, SAND80-1258, Sandia National Laboratories, Albuquerque, NM, 50 p.
2. Wawersik, W. R. and D. W. Hannum (1980), "Mechanical Behavior of New Mexico Rock Salt in Triaxial Compression up to 200°C," J. Geophys. Res., 85, B2, 891-900.
3. Schuler, K. W. (1978), "Lateral Deformation Gauge for Rock Mechanics Testing," Exp. Mech., 18, 12.
4. Wawersik, W. R. (1979), "Indirect Deformation (Strain) Measurements and Calibrations in Sandia Triaxial Apparatus for Testing to 250°C," Sandia National Laboratories Report, SAND79-0114, Sandia National Laboratories, Albuquerque, NM, 44 p.
5. Wawersik, W. R., D. W. Hannum and H. S. Lauson (1980), "Compression and Extension Data for Dome Salt from West Hackberry, Louisiana," Sandia National Laboratories Report, SAND79-0668, Sandia National Laboratories, Albuquerque, NM, 34 p.
6. Wawersik, W. R., D. J. Holcomb, D. W. Hannum and H. S. Lauson (1980), "Quasi-Static and Creep Data for Dome Salt from Bryan Mound, Texas," Sandia National Laboratories Report, SAND80-1434, Sandia National Laboratories, Albuquerque, NM, 36 p.

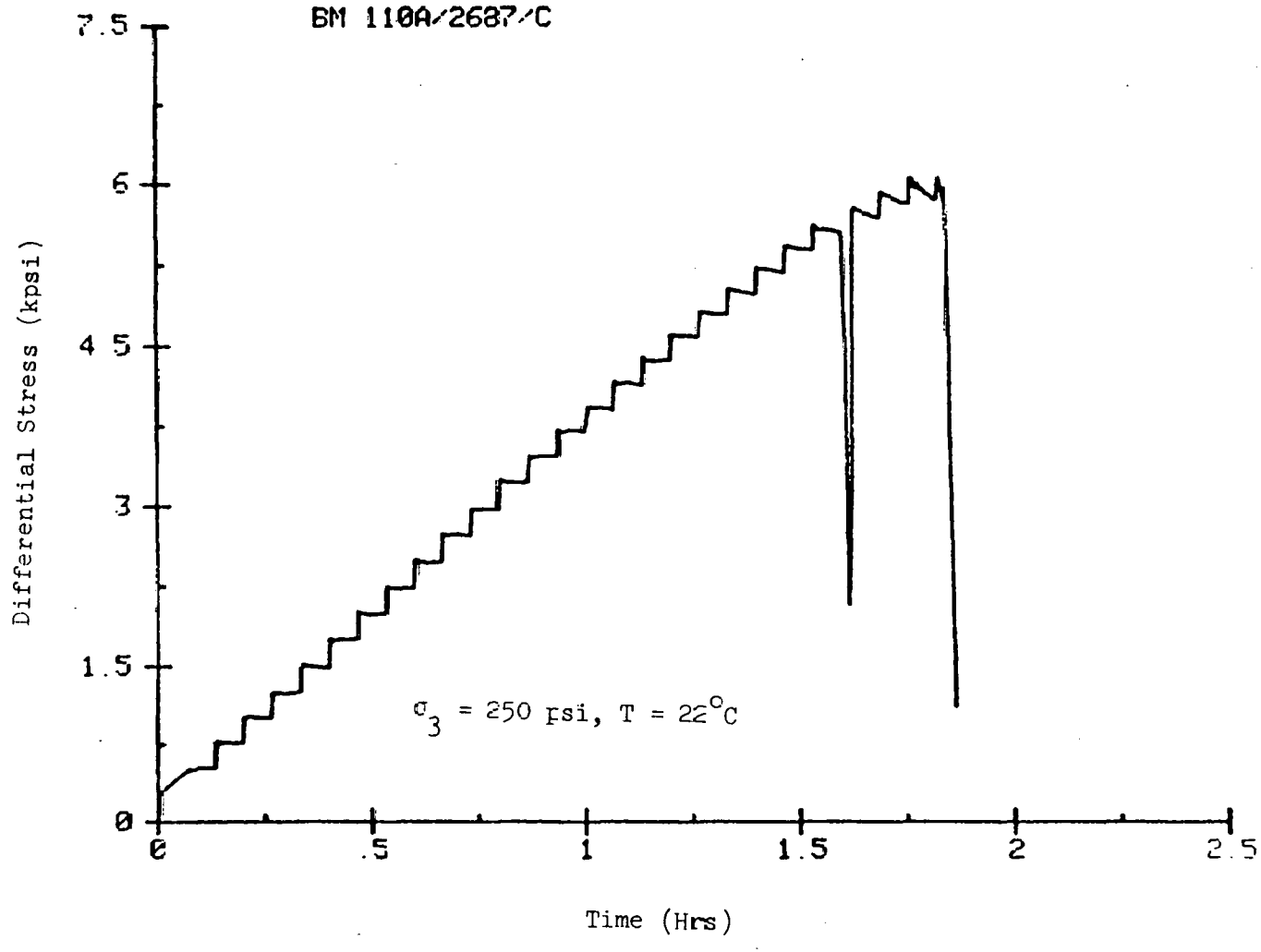


Figure 1: Differential stress-time curve for sample BM 110A/2687 deformed in compression at 250 psi and 22°C

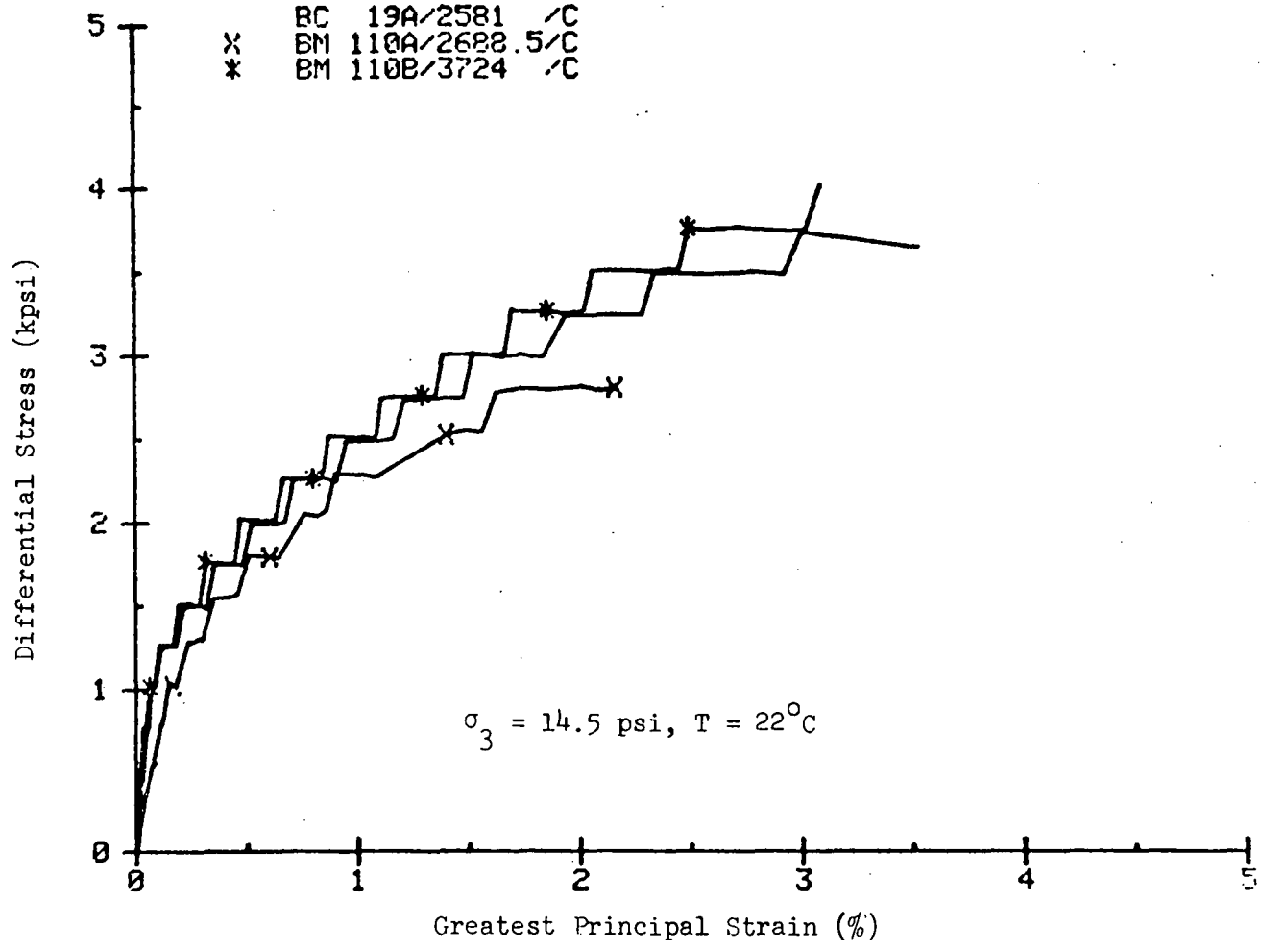


Figure 2A: Differential stress-greatest principal strain curves for samples BC 19A/2581, BM 110A/2688.5 and BM 110B/3724 deformed in compression at 14.5 psi and 22°C.

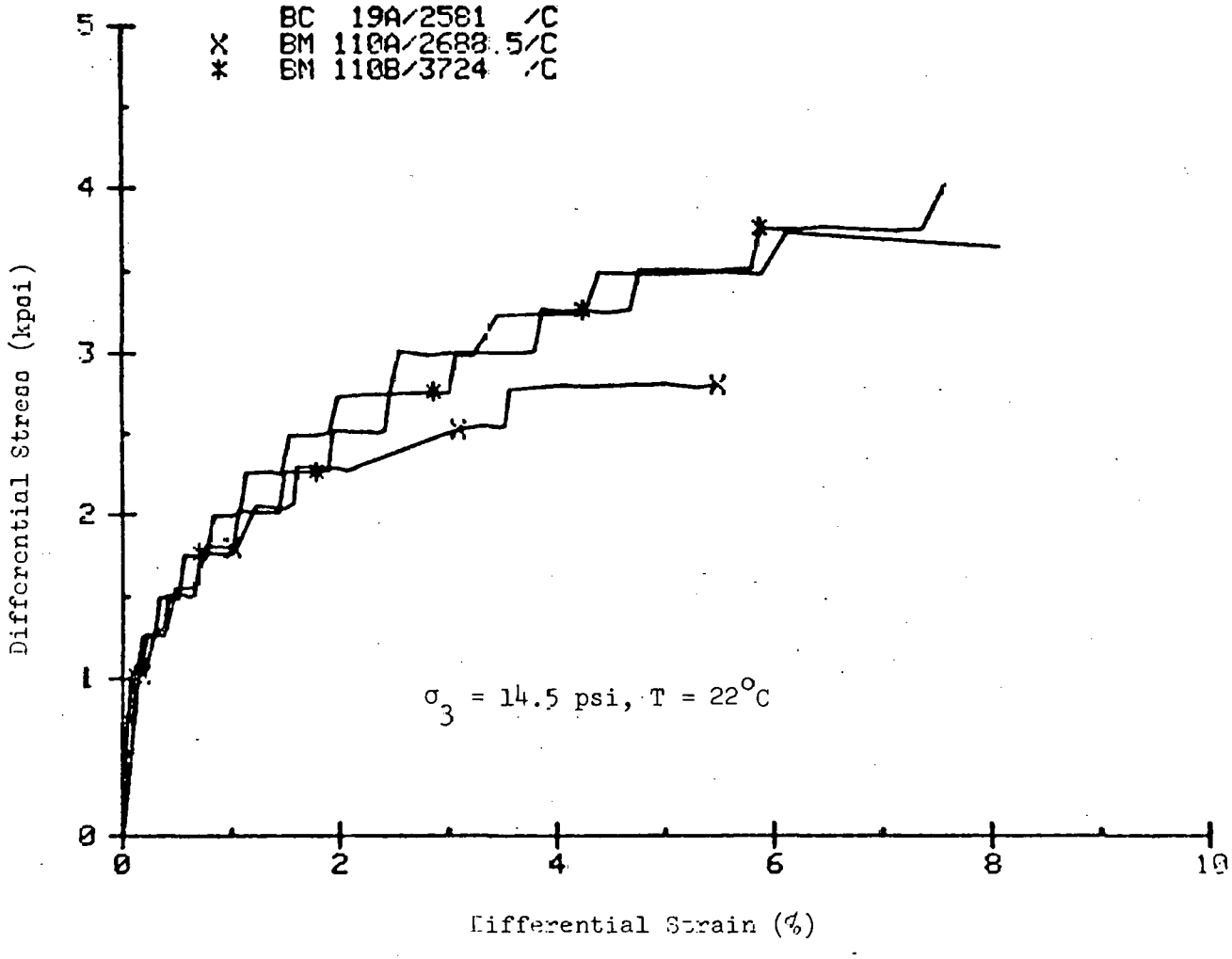


Figure 2B: Differential stress-differential strain curves for samples BC 19A/2581, BM 110A/2688.5 and BM 110B/3724 deformed in compression at 14.5 psi and 22°C.

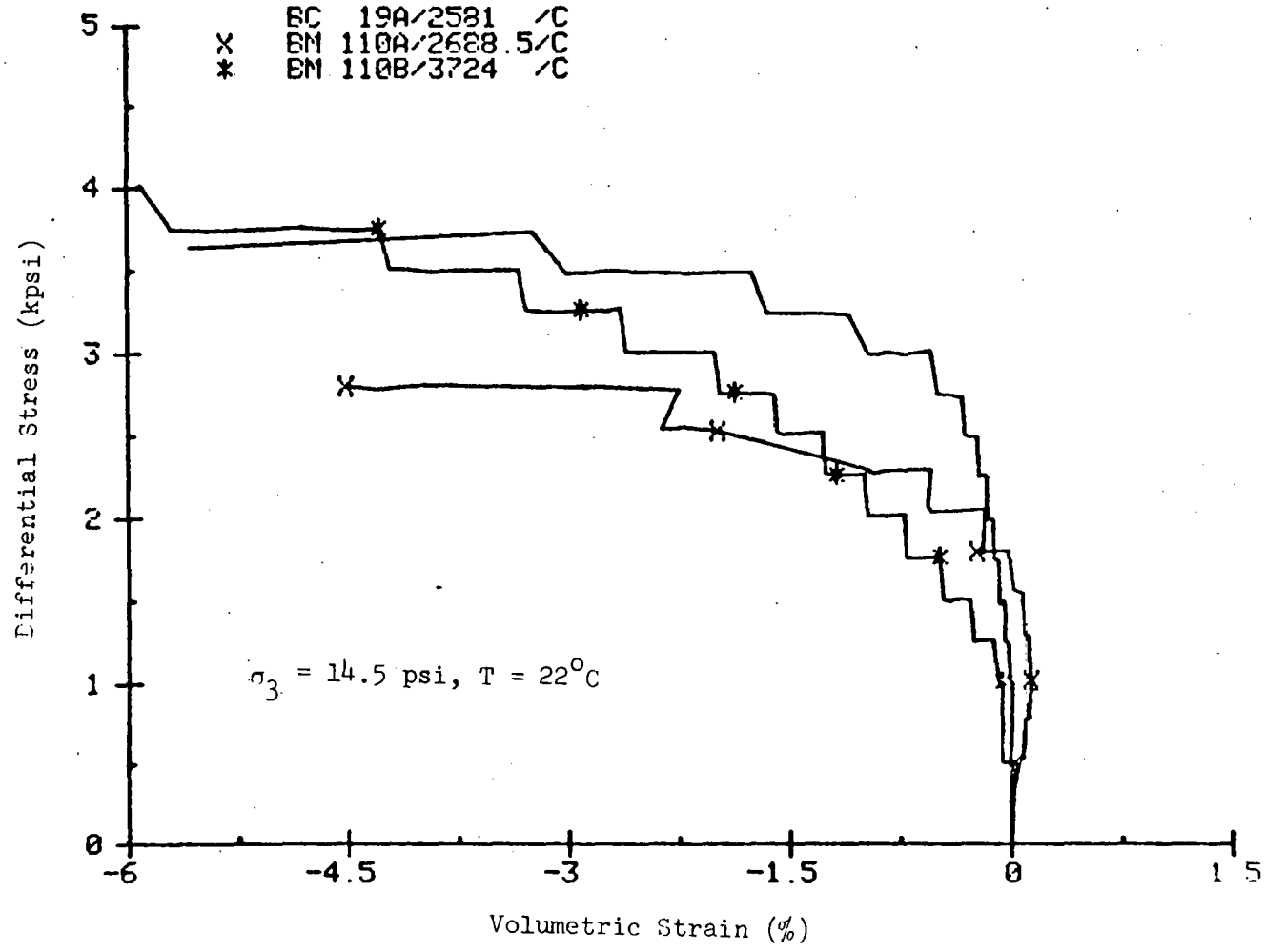


Figure 2C: Differential stress-volumetric strain curves for samples BC 19A/2581, BM 110A/2688.5 and BM 110B/3724 deformed in compression at 14.5 psi and 22°C.

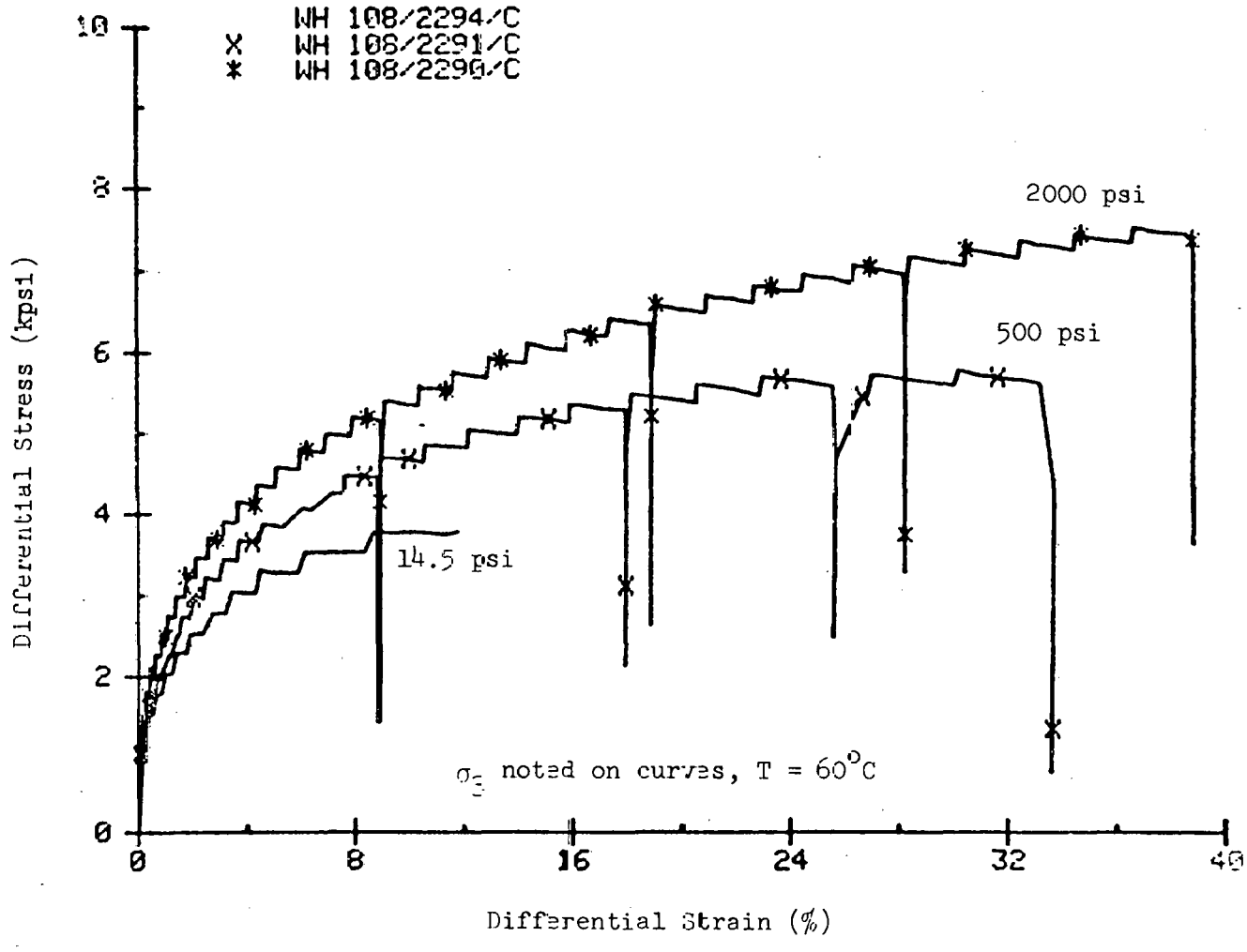


Figure 3A: Differential stress-differential strain curves for samples WH 108/2294, WH 108/2291 and WH 108/2290 deformed in compression at 14.5, 500, 2000 psi and 60°C.

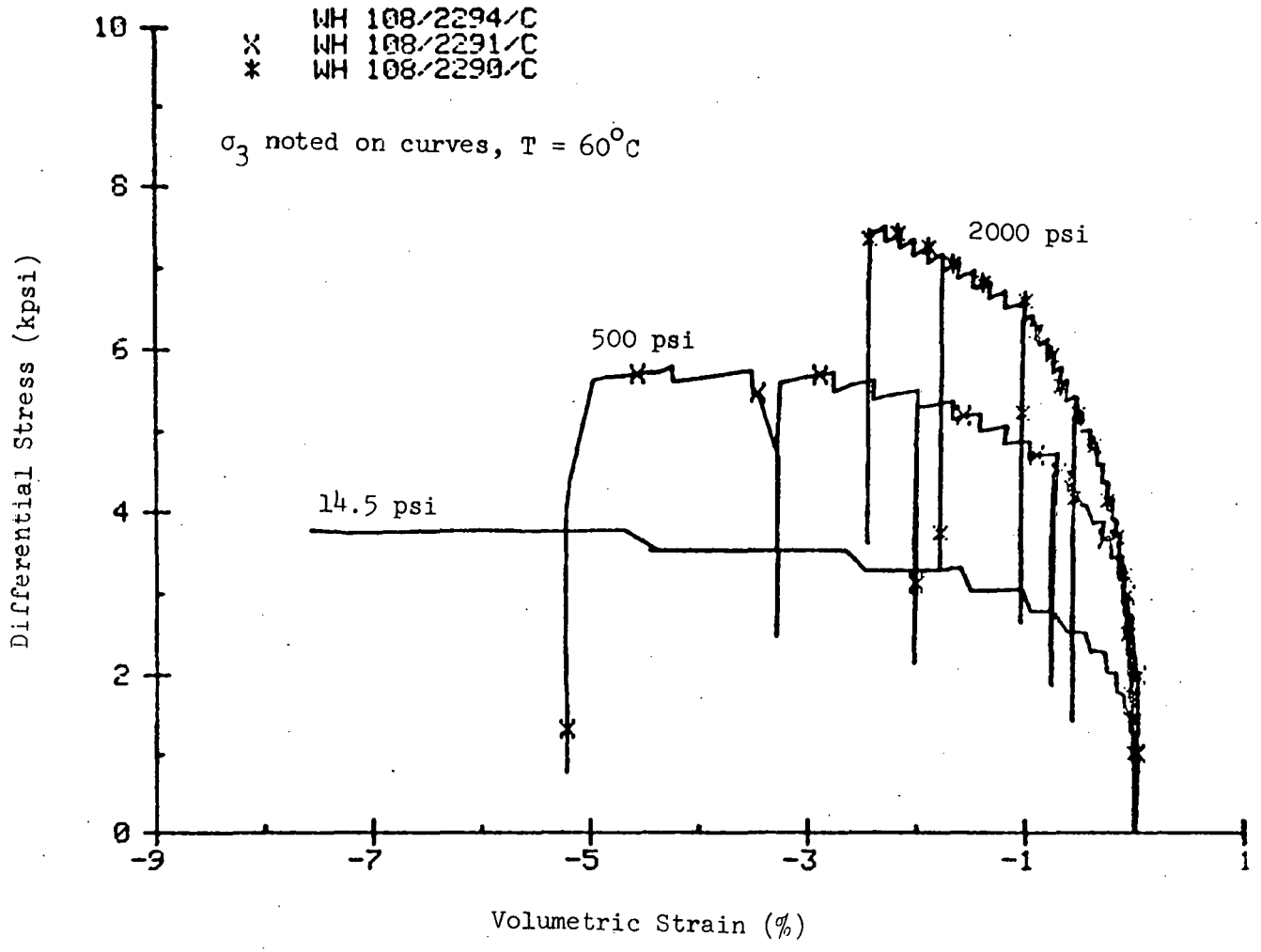


Figure 3B: Differential stress-volumetric strain curves for samples WH 108/2294, WH 108/2291 and WH 108/2290 deformed in compression at 14.5, 500, 2000 psi and 60°C.

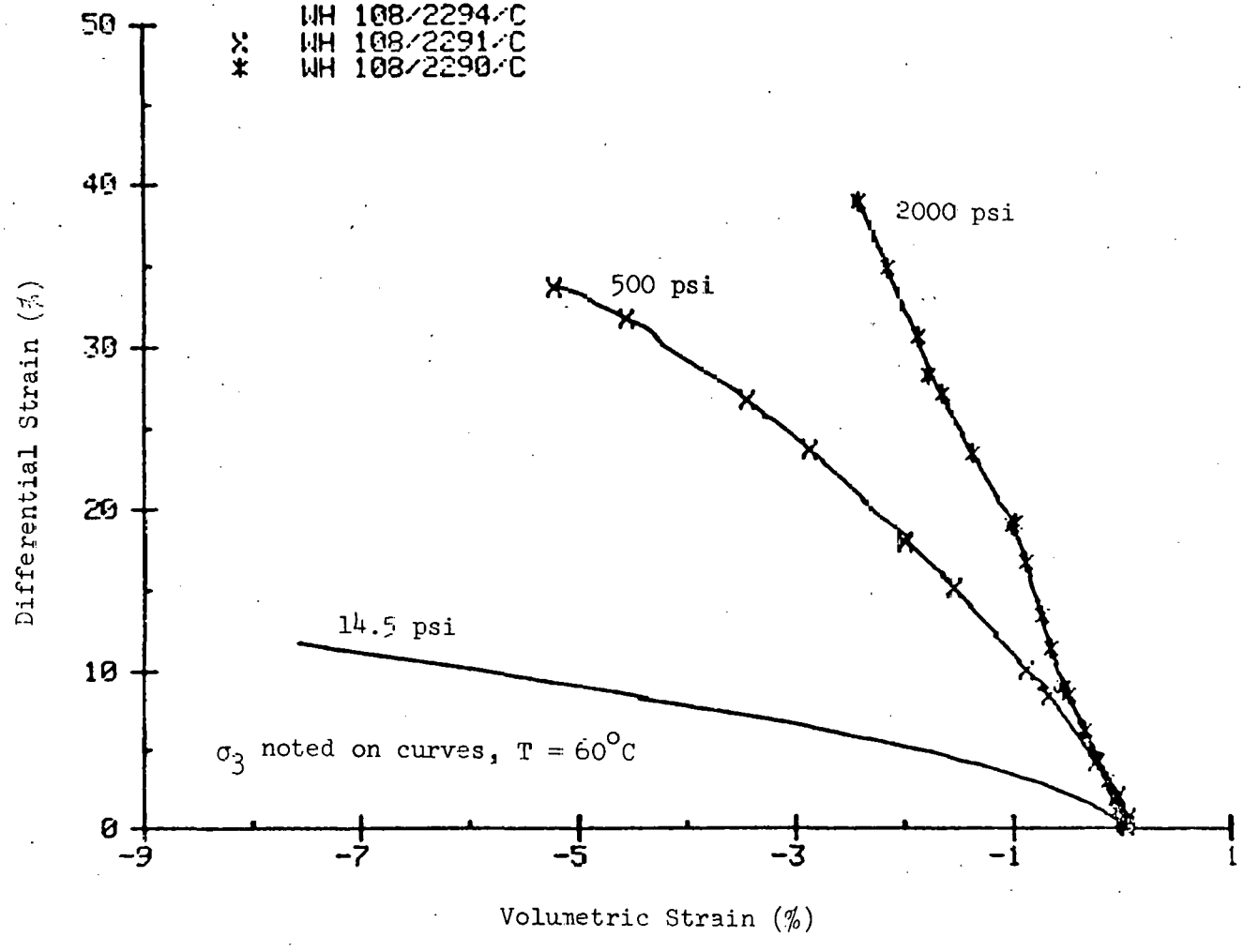


Figure 30: Differential strain-volumetric strain curves for samples WH 108/2294, WH 108/2291 and WH 108/2290 deformed in compression at 14.5, 500, 2000 psi and 60°C.

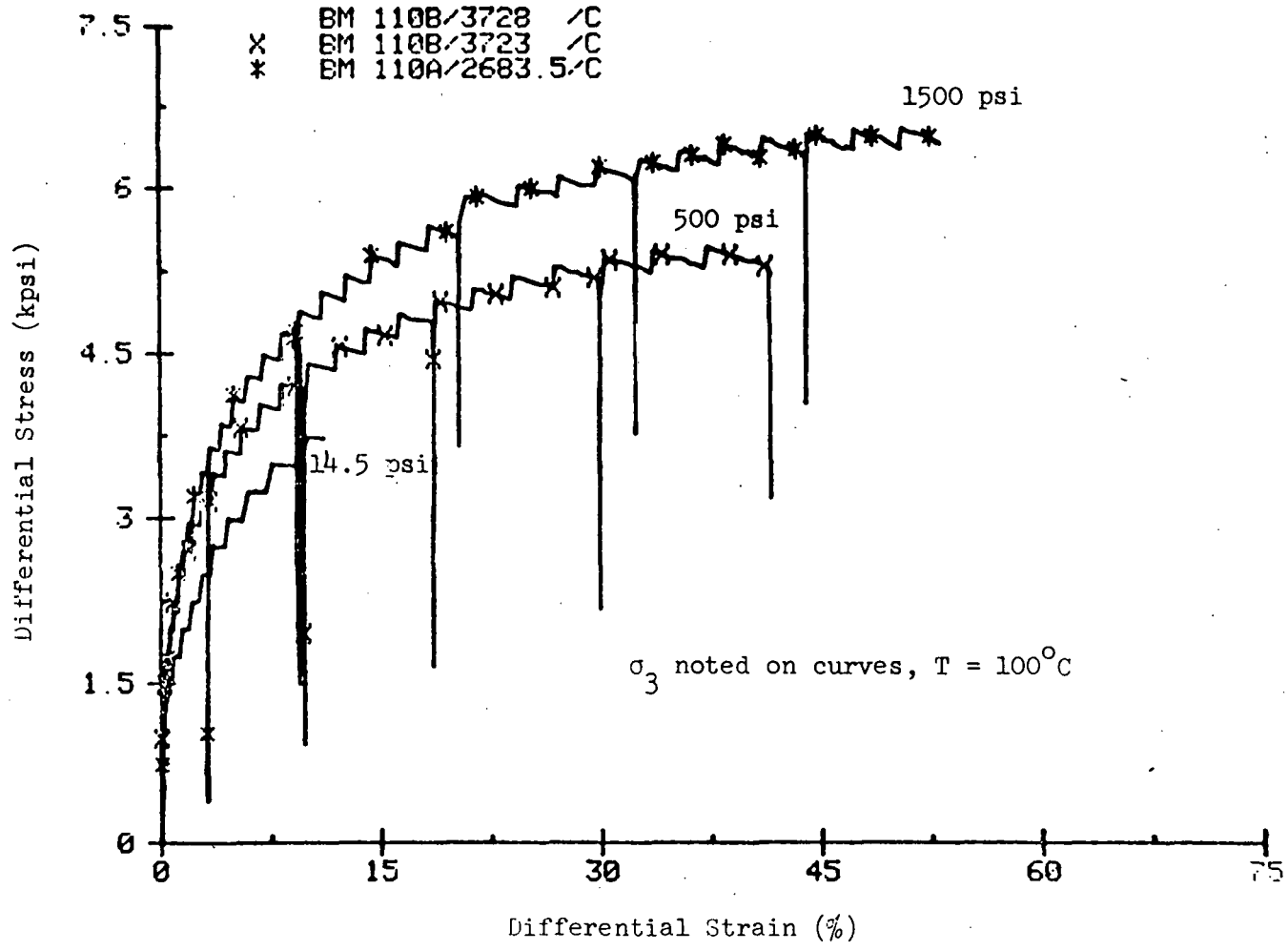


Figure 4A: Differential stress-differential strain curves for samples BM 110B/3728, BM 110B/3723 and BM 110A/2683.5 deformed in compression at 14.5, 500, 1500 psi and 100°C.

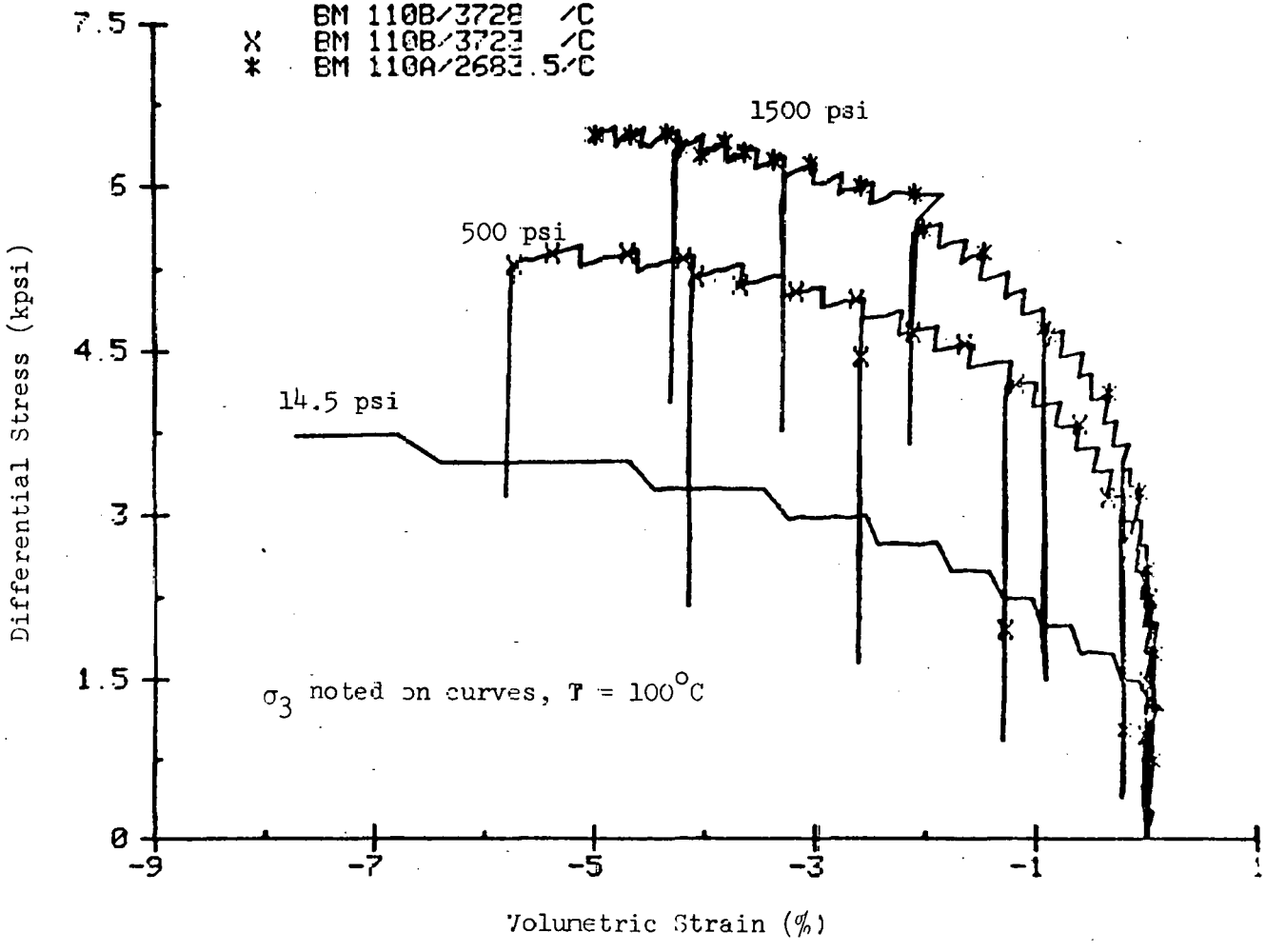


Figure 43: Differential stress-volumetric strain curves for samples BM 110B/3728, BM 110B/3723 and BM 110A/2683.5 deformed in compression at 14.5, 500, 1500 psi and 100°C.

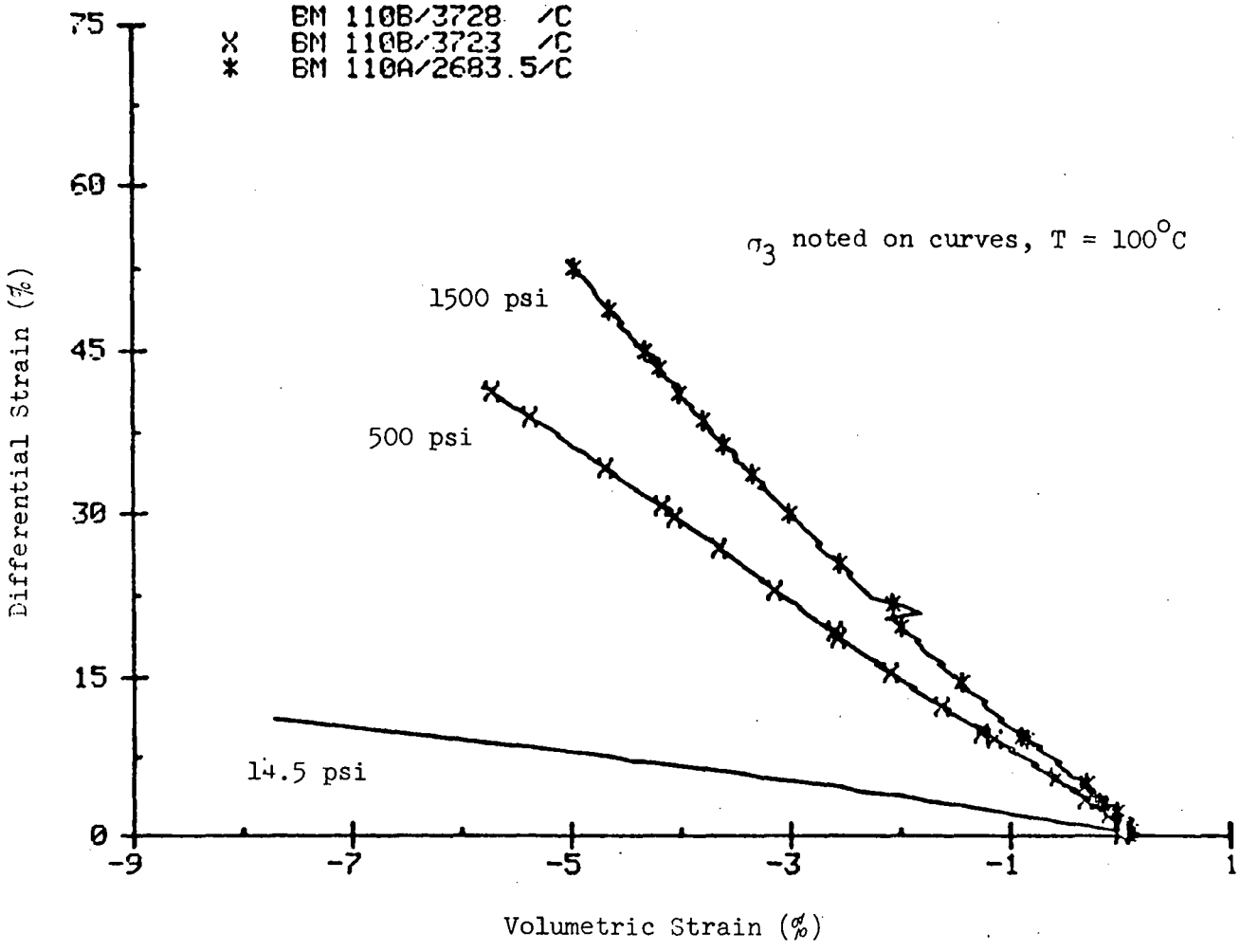


Figure 4C: Differential strain-volumetric strain curves for samples BM 110B/3728, BM 110B/3723 and BM 110A/2683.5 deformed in compression at 14.5, 500, 1500 psi and 100°C.

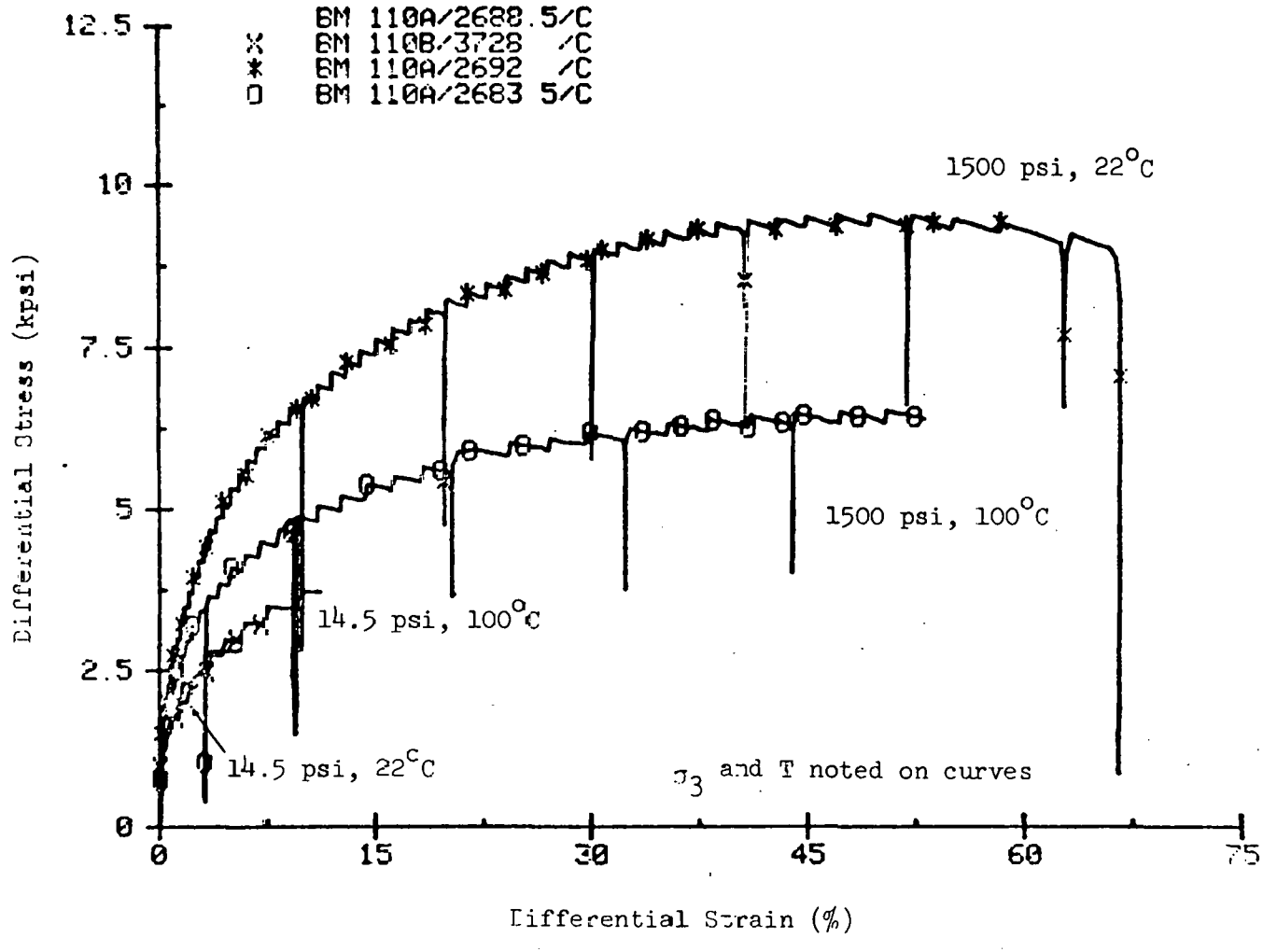


Figure 5A: Differential stress-differential strain curves for samples BM 110A/2688.5 and BM 110B/3728 deformed in compression at 14.5 psi and 22, 100°C; and BM 110A/2692 and BM 110A/2683.5 deformed in compression at 1500 psi and 22, 100°C.

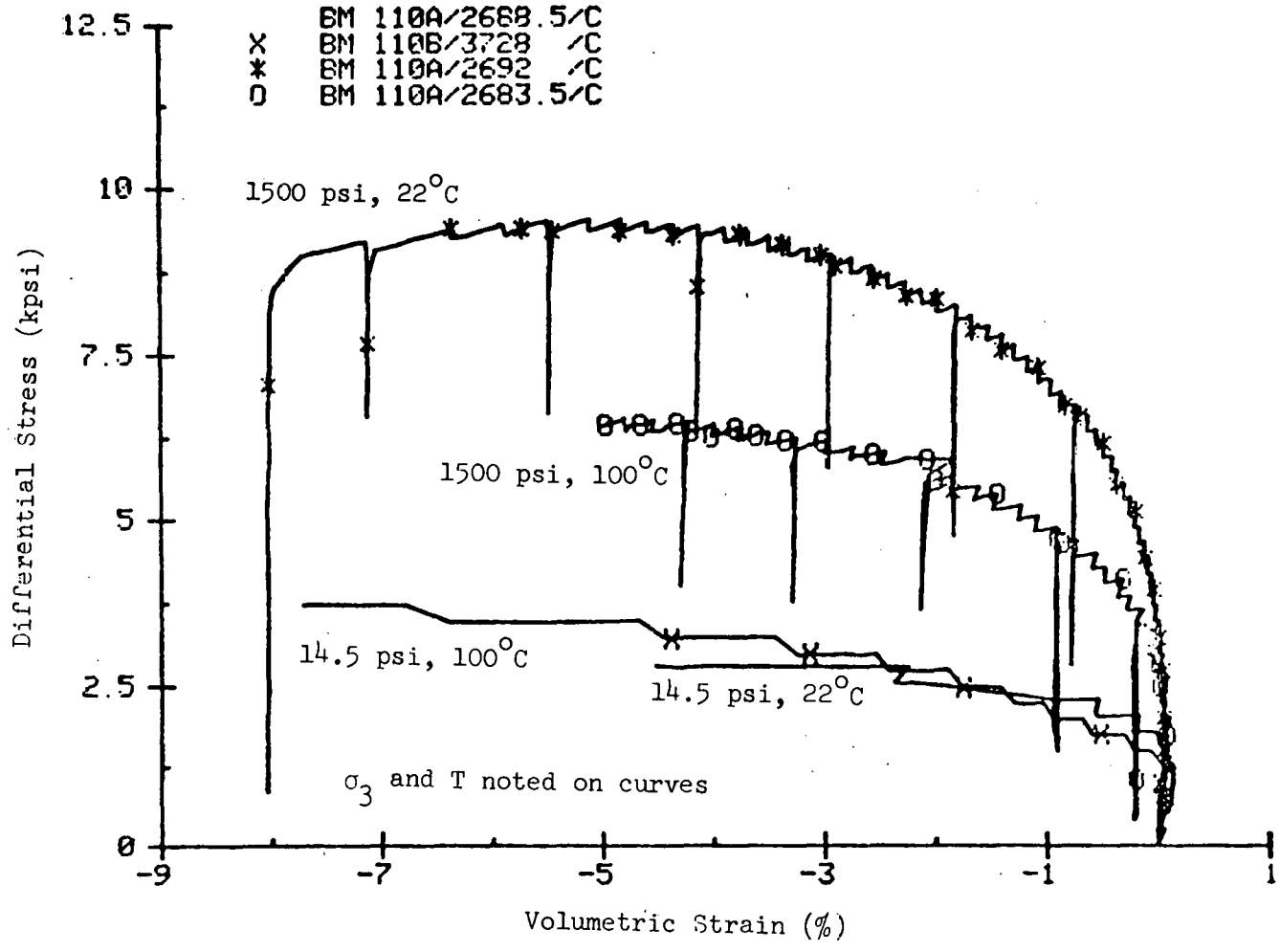


Figure 5B: Differential stress-volumetric strain curves for samples BM 110A/2688.5 and BM 110B/3728 deformed in compression at 14.5 psi and 22, 100°C; and BM 110A/2692 and BM 110A/2683.5 deformed in compression at 1500 psi and 22, 100°C.

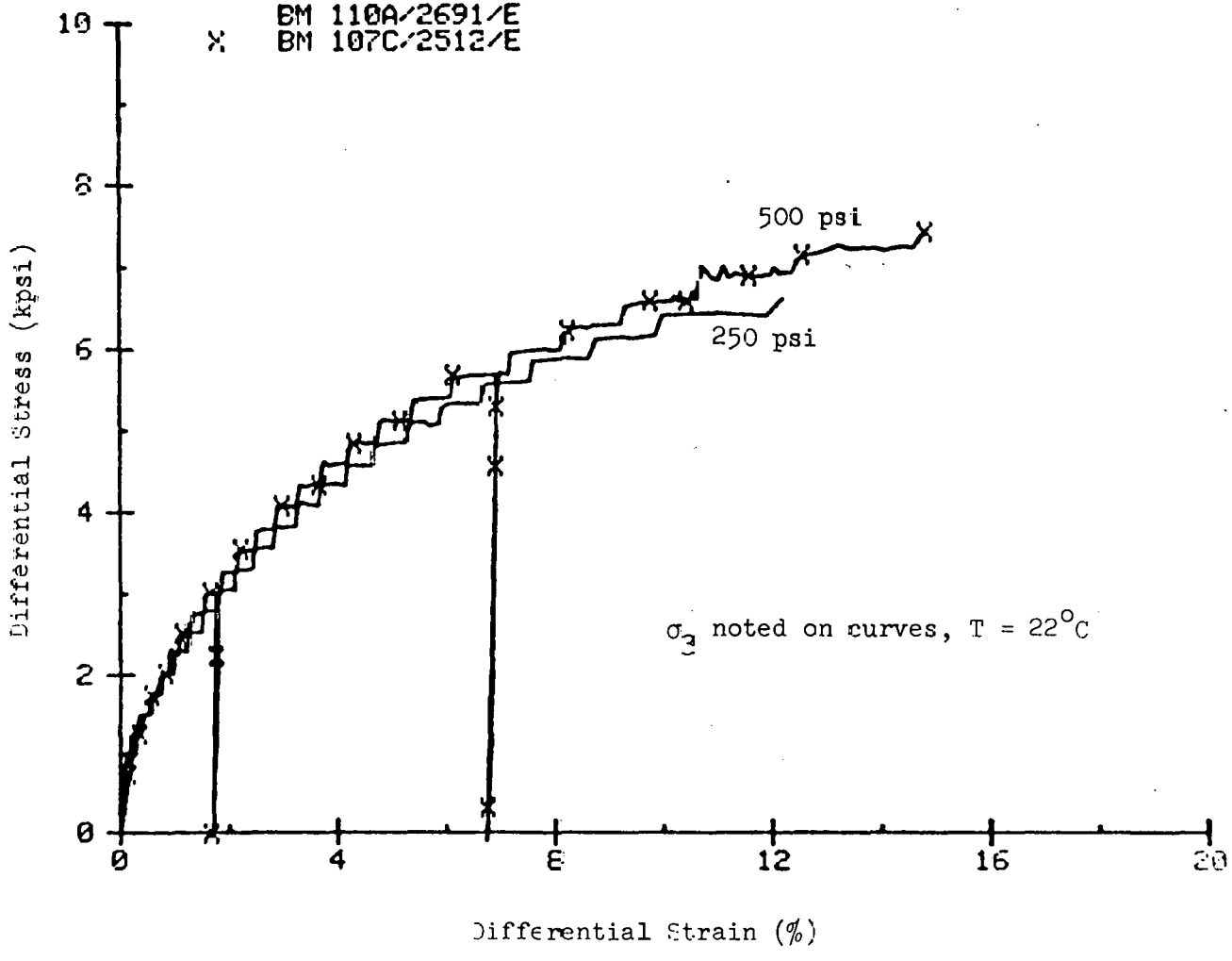


Figure 6A: Differential stress-differential strain curves for samples BM 110A/2691 and BM 107C/2512 deformed in extension at 25C, 50C psi and 22°C.

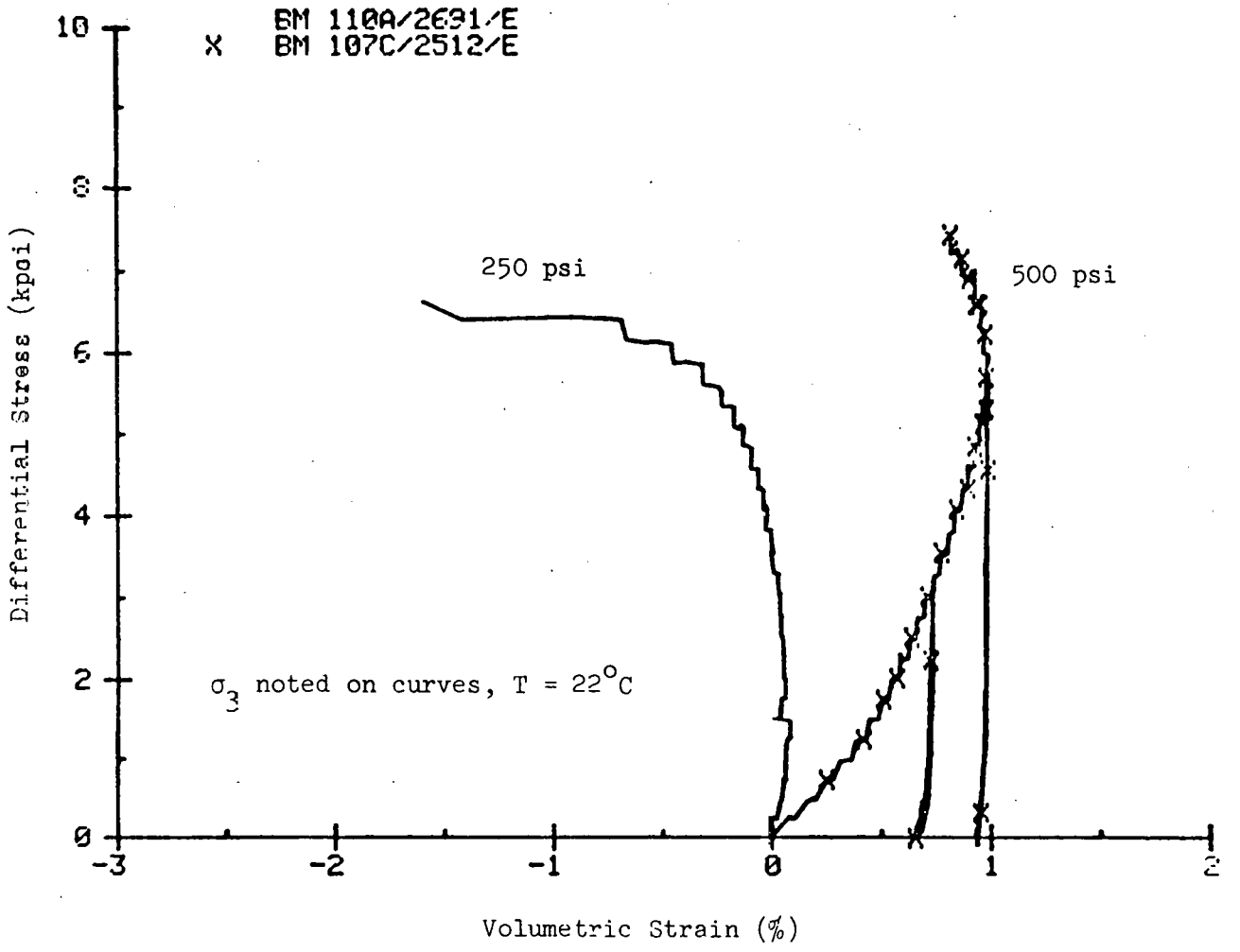


Figure 6B: Differential stress-volumetric strain curves for samples BM 110A/2691 and BM 107C/2512 deformed in extension at 250, 500 psi and 22°C.

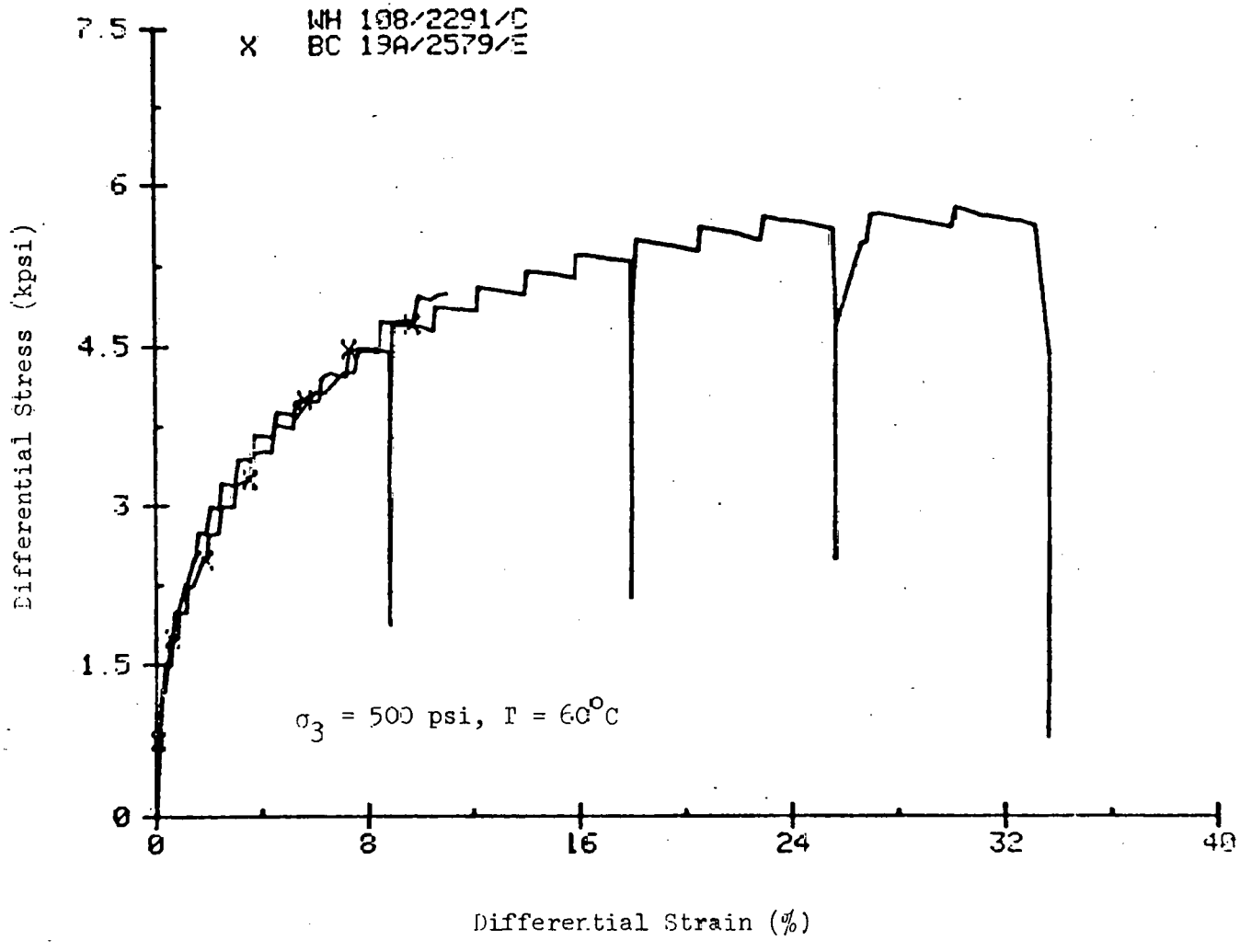


Figure 7A: Differential stress-differential strain curves for sample WH 108/2291 deformed in compression and BC 19A/2579 deformed in extension at 500 psi and 60°C.

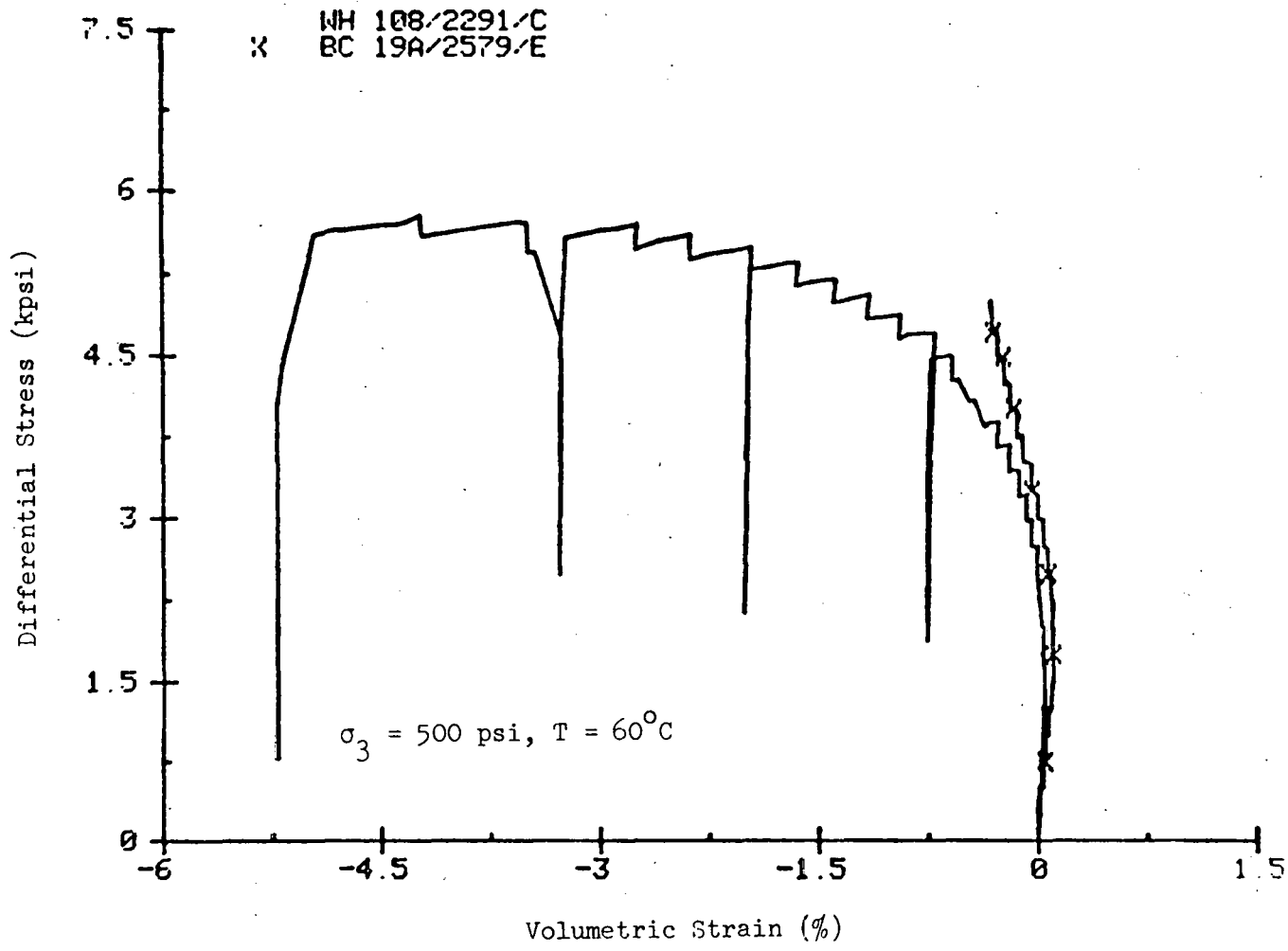


Figure 7B: Differential stress-volumetric strain curves for sample WH 108/2291 deformed in compression and BC 19A/2579 deformed in extension at 500 psi and 60°C.

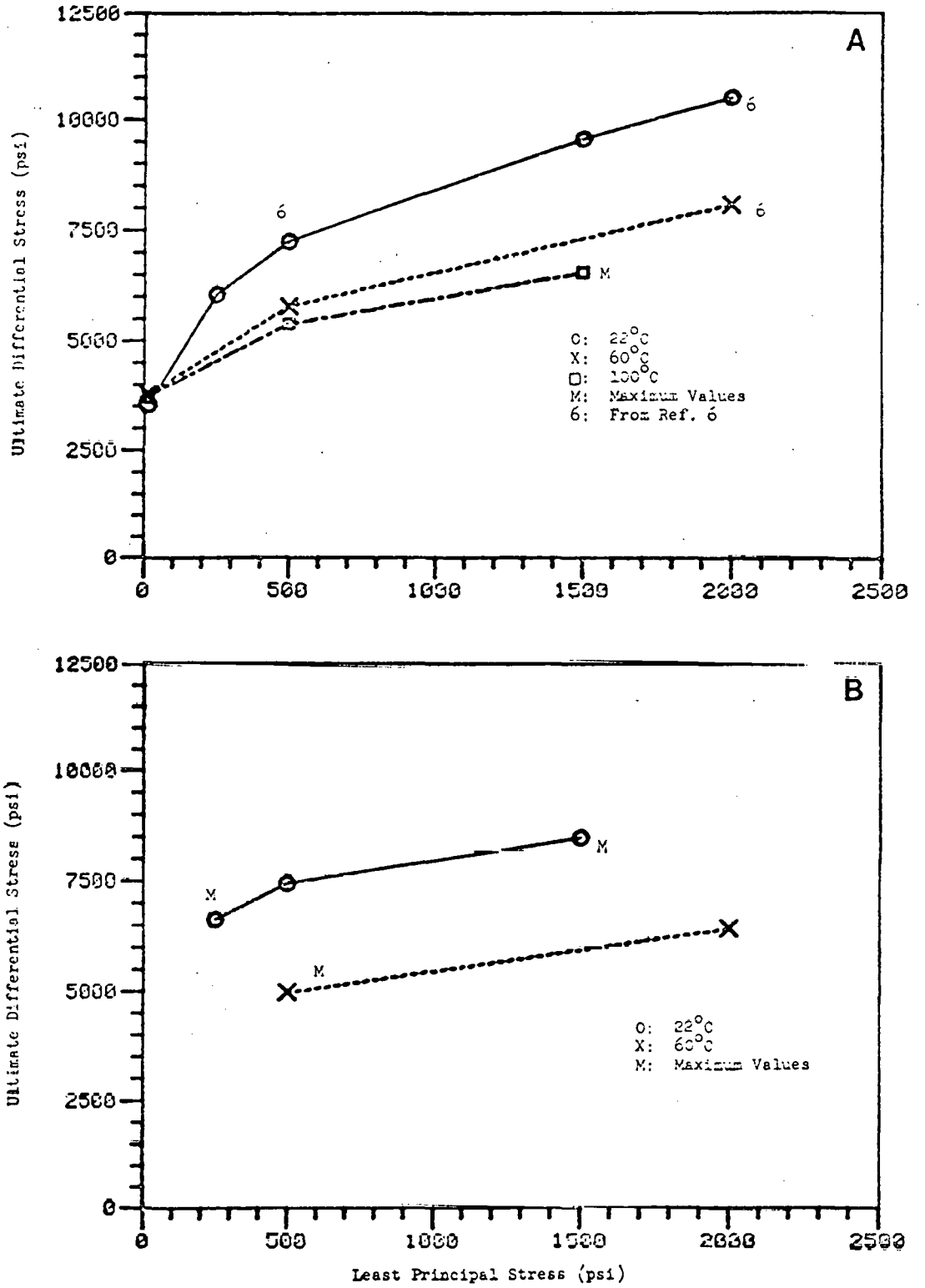


Figure 8: Ultimate differential stress-least principal stress plots for samples deformed in (A) compression and (B) extension.

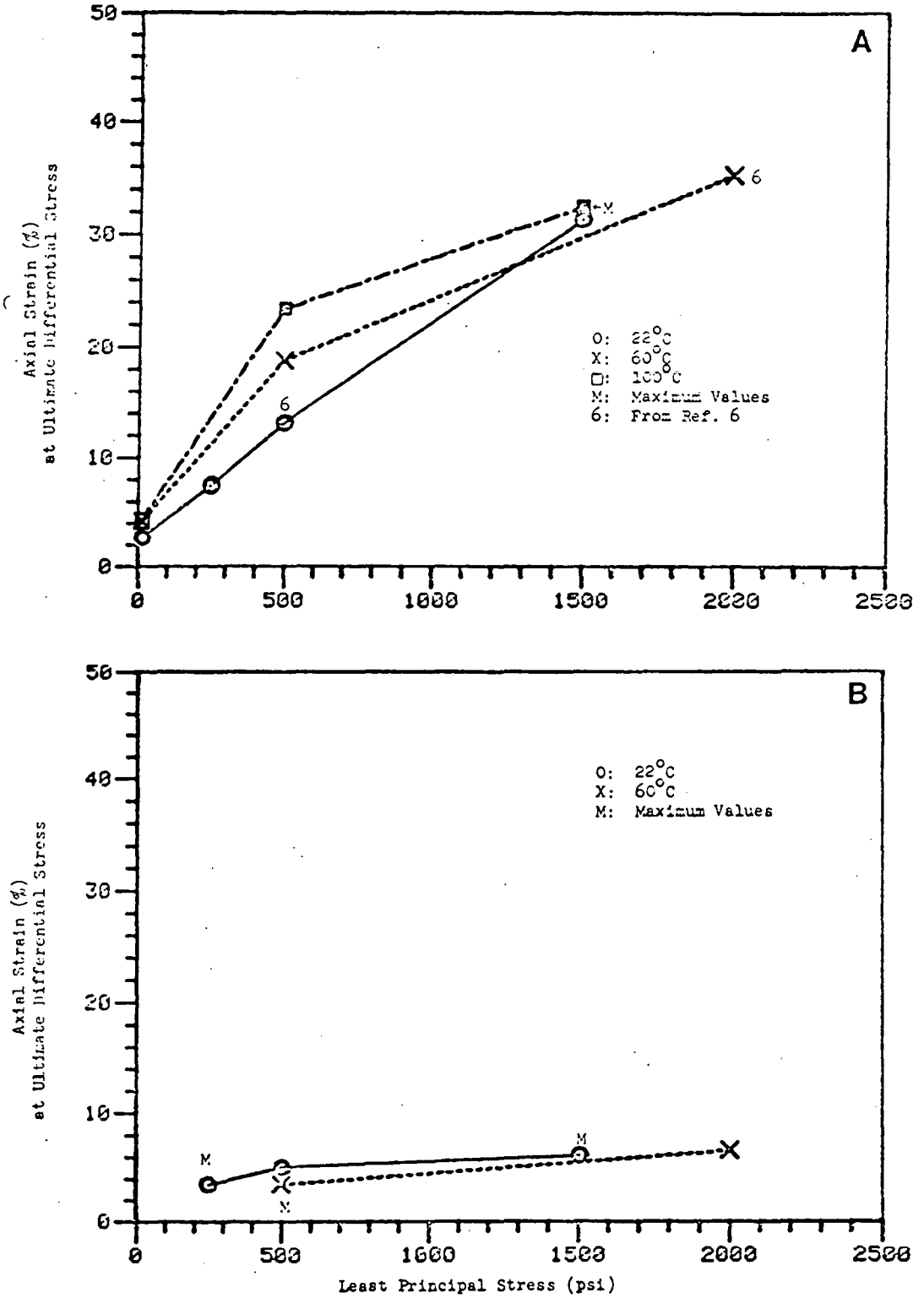


Figure 9: Axial strain at $(\sigma_1 - \sigma_3)_u$-least principal stress plots for samples deformed in (A) compression and (B) extension.

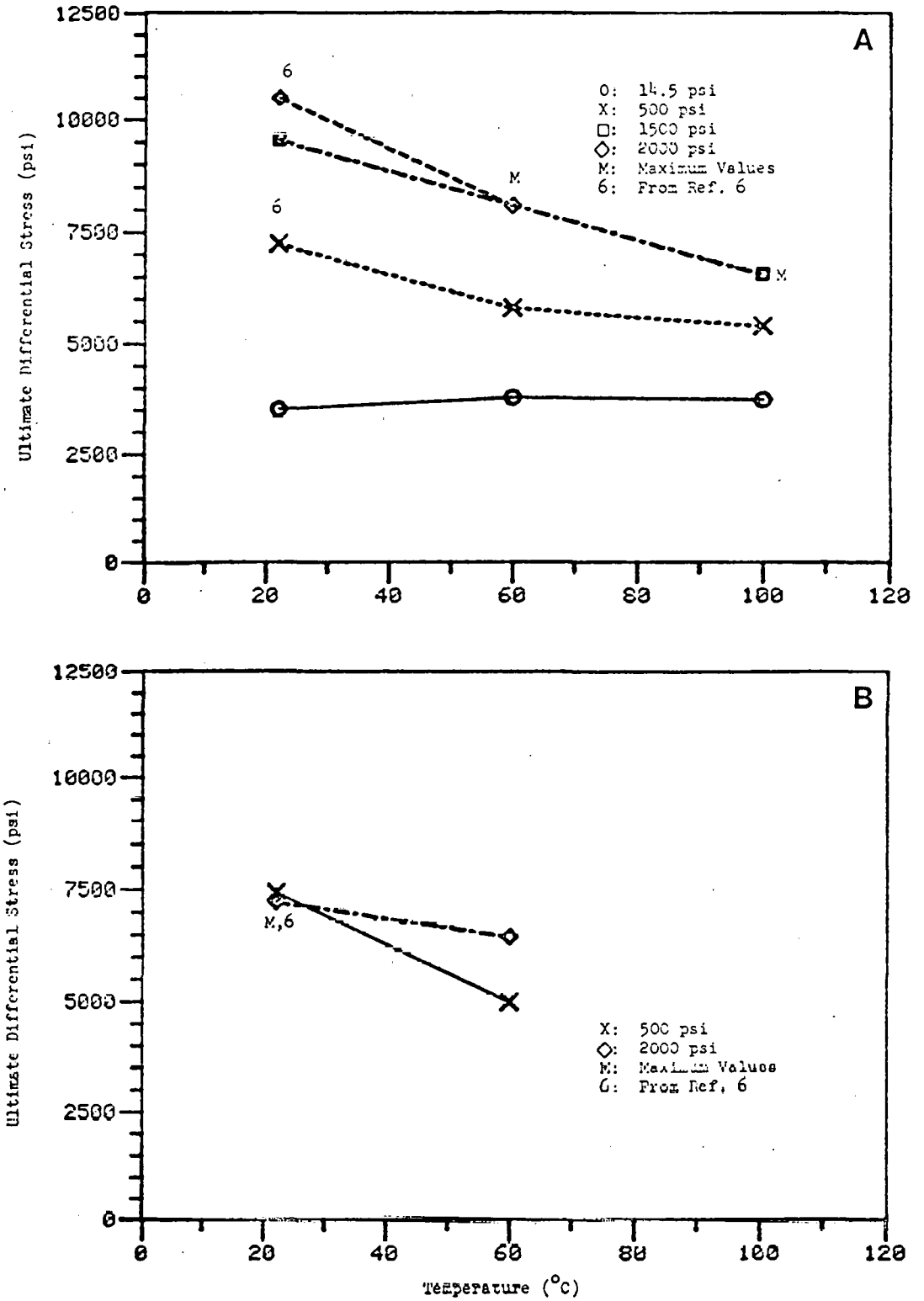


Figure 10: Ultimate differential stress-temperature plots for samples deformed in (A) compression and (B) extension.

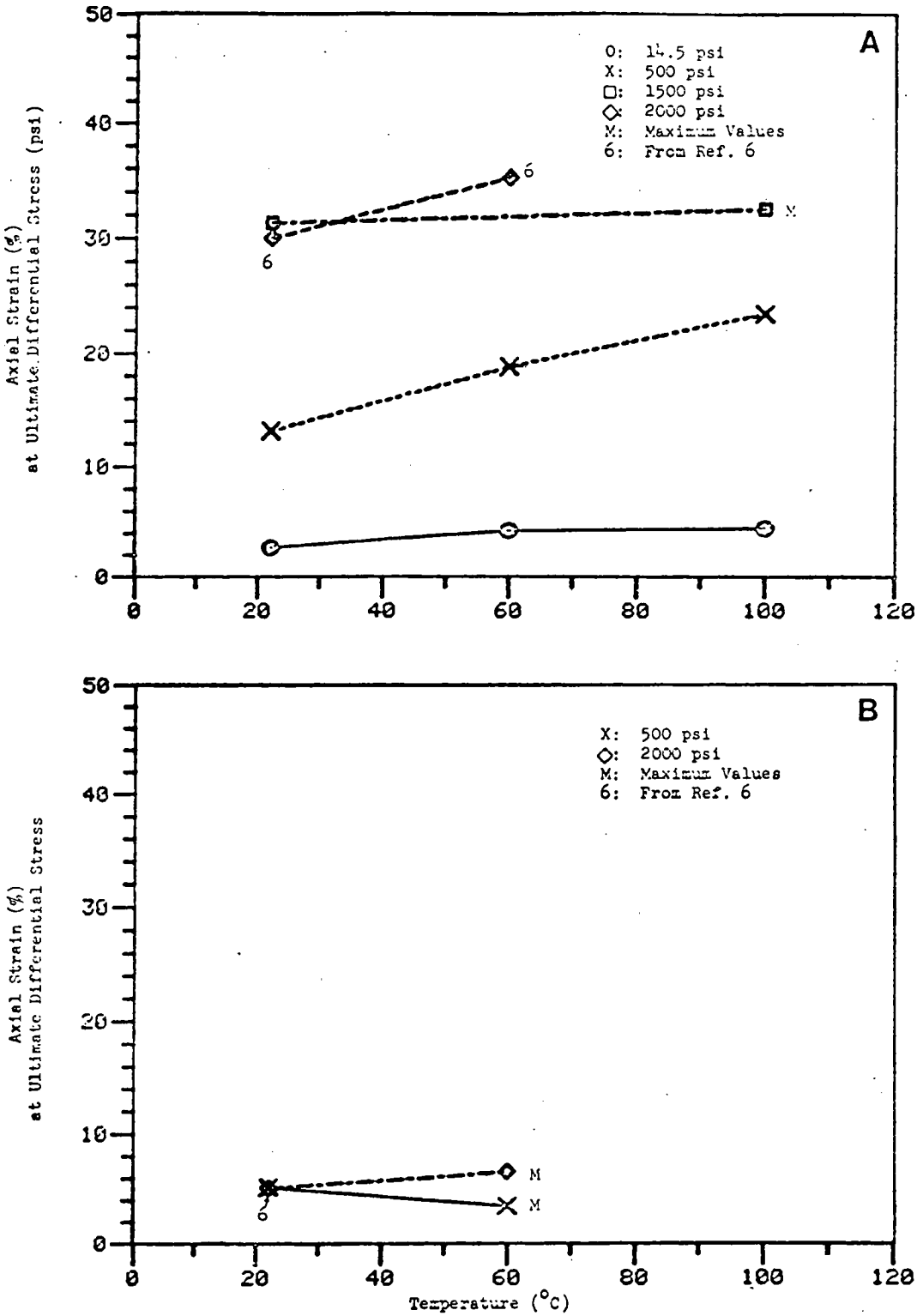


Figure 11: Axial strain at $(\sigma_1 - \sigma_3)_u$ temperature plots for samples deformed in (A) compression and (B) extension.

Distribution:

US Department of Energy
Strategic Petroleum Reserve
Project Management Office
900 Commerce Road East
New Orleans, LA 70123
Attn: E. E. Chapple (5)
C. C. Johnson
G. A. Stafford
C. L. Steinkamp

US Department of Energy
Strategic Petroleum Reserve
1000 Independence Avenue SW
Washington, DC 20585
Attn: L. Pettis
R. Smith

Aerospace Corporation
880 Commerce Road West, Suite 300
New Orleans, LA 70123
Attn: K. Henrie
R. Merkle

Aerospace Corporation
P. O. Box 92957
Los Angeles, CA 90009
Attn: G. F. Kuncir

Jacobs/D'Appolonia Engineers
6226 Jefferson Hwy., Suite B
New Orleans, LA 70123
Attn: H. Kubicek
P. Campbell

David K. Parrish
RE/SPEC, Inc.
P. O. Box 725
Rapid City, SD 57701

John W. Handin
Center for Tectonophysics
Texas A&M University
College Station, TX 77843

Neville L. Carter
Department of Geophysics
Texas A&M University
College Station, TX 77843

4000 A. Narath
4500 E. H. Beckner
4512 T. O. Hunter
4512 R. V. Matalucci
4512 D. E. Munson
4540 M. L. Kramm
4543 J. F. Ney
4543 R. R. Beasley
5500 O. E. Jones
5510 D. B. Hayes
5520 T. B. Lane
5521 R. D. Krieg
5522 D. S. Preece
5530 W. Herrmann
5532 B. M. Butcher
5532 D. W. Hannum
5532 R. H. Price (15)
5532 W. R. Wawersik (5)
5532 D. H. Zeuch
5532 J. A. Zirzow
3141 L. J. Erickson (5)
3151 W. L. Garner (3)
3154-3 C. Dalin (25)
For: DOE/TIC
(Unlimited Release)
8214 M. A. Pound

| Org. | Bldg. | Name | Rec'd by | Org. | Bldg. | Name | Rec'd by |
|---|---|---|---|---|---|---|---|
| | | | | | | | |
| | | | | | | | |
| | | | | | | | |
| | | | | | | | |
| | | | | | | | |
| | | | | | | | |
| | | | | | | | |
| | | | | | | | |
| | | | | | | | |
| | | | | | | | |
| | | | | | | | |
| | | | | | | | |
| | | | | | | | |
| | | | | | | | |
| | | | | | | | |

Sandia National Laboratories